

Effects of ice deformation on Røthlisberger channels and implications for transitions in subglacial hydrology

COLIN R. MEYER,¹ MATHEUS C. FERNANDES,¹ TIMOTHY T. CREYTS,²
JAMES R. RICE^{1,3}

¹John A. Paulson School of Engineering and Applied Sciences, Harvard University, Cambridge, MA 02138, USA

²Lamont-Doherty Earth Observatory of Columbia University, Palisades, NY 10964, USA

³Department of Earth and Planetary Sciences, Harvard University, Cambridge, MA 02138, USA

Correspondence: Colin R. Meyer <colinmeyer@gmail.com>

ABSTRACT. Along the base of glaciers and ice sheets, the sliding of ice over till depends critically on water drainage. In locations where drainage occurs through Røthlisberger channels, the effective pressure along the base of the ice increases and can lead to a strengthening of the bed, which reduces glacier sliding. The formation of Røthlisberger channels depends on two competing effects: (1) melting from turbulent dissipation opens the channel walls and (2) creep flow driven by the weight of the overlying ice closes the channels radially inward. Variation in downstream ice velocity along the channel axis, referred to as an antiplane shear strain rate, decreases the effective viscosity. The softening of the ice increases creep closure velocities. In this way, even a modest addition of antiplane shear can double the size of the Røthlisberger channels for a fixed water pressure or allow channels of a fixed radius to operate at lower effective pressure, potentially decreasing the strength of the surrounding bed. Furthermore, we show that Røthlisberger channels can be deformed away from a circular cross section under applied antiplane shear. These results can have broad impacts on sliding velocities and potentially affect the total ice flux out of glaciers and ice streams.

KEYWORDS: glacier hydrology, glacier mechanics, ice rheology, ice streams, subglacial processes

1. INTRODUCTION

Observations show a definitive link between subglacial hydrology and glacier sliding (Iken and Bindschadler, 1986; Kamb, 1987; Fischer and Clarke, 1997). Furthermore, observations show that the style of subglacial drainage influences sliding speed (Kamb and others, 1985; Brugman, 1986; Raymond, 1987). There are generally thought to be two modes of drainage in subglacial hydrology: (1) concentrated channels such as Røthlisberger channels (R-channels) incised into the ice (Røthlisberger, 1972; Shreve, 1972; Weertman, 1972) or Nye channels eroded into hard bedrock (Weertman, 1972; Nye, 1973; Walder and Hallet, 1979), that operate at low water pressure relative to the overburden pressure of the overlying ice, (2) distributed water systems, including a network of linked cavities (Lliboutry, 1979; Anderson and others, 1982; Walder, 1986) or canals (Walder and Fowler, 1994; Fowler and Ng, 1996; Ng, 1998) connected by thin sheets of water at high pressure (Flowers and Clarke, 2002a; Creyts and Schoof, 2009; Hewitt, 2011).

In water-saturated basal sediments, glacier sliding can also occur by till deformation (Alley and others, 1986). Till of low permeability, high water content and high pore pressure, commonly underlies regions of fast flow of glaciers and ice sheets (Clarke and others, 1984; Blankenship and others, 1986; Kamb, 2001). Observations indicate that till typically behaves as a perfectly plastic material with a yield stress that depends on the effective pressure, the overburden pressure of the ice less the pore pressure (Kamb, 1991; Tulaczyk and others, 2000; Cuffey and Paterson, 2010). Changes in till effective pressure often occur by flow in subglacial hydrology systems instead of Darcy flow because the permeability of till

is too small (Boulton and others, 1974; Clarke, 1987; Engelhardt and others, 1990). Thus, water flow through subglacial hydrologic systems along the ice/till interface can locally depress the till yield stress, leading to till deformation and glacier sliding.

A sliding law that connects the basal shear stress τ_b to the basal sliding velocity u_b and effective pressure N at the bed is

$$\tau_b = \frac{\xi N^c u_b^d}{|u_b|}, \quad (1)$$

where ξ is a constant of proportionality. The effective pressure,

$$N = \sigma_o - p_w, \quad (2)$$

is given as hydrostatic ice overburden pressure σ_o less the water pressure p_w , and the exponents are $c \geq 0$, $d \geq 1$ (Lliboutry, 1968; Budd and others, 1979; Schoof, 2005). This sliding law indicates that increasing the effective pressure along the basal interface decreases the basal sliding velocity for a constant basal shear stress (Schoof, 2010a, b; Hewitt, 2013). In this way, basal sliding velocities are larger over distributed hydrologic systems, which operate at lower effective pressure than channels. Thus, a switch to a channelised drainage system strengthens the bed. For hydrologically controlled surging glaciers, such as the hundredfold speedup of the Variegated Glacier in Alaska, which occurs about every two decades (Eisen and others, 2005), a transition from a distributed system to channelised drainage increases the strength of the bed and can terminate a surge (Fowler, 1987; Kamb, 1987; Björnsson, 1998).

Transitions in sliding velocity across ice-stream margins can also be related to subglacial hydrology. Surface velocity data show that ice drainage in Antarctica is not uniform but rather focused in regions of fast-flowing ice called ice streams (Joughin and Tulaczyk, 2002; Joughin and others, 2002; Rignot and others, 2011). Satellite altimetry data reveal connected subglacial hydrological systems beneath the Siple Coast Ice Streams with prominent subglacial lakes along the margins of the Whillans Ice Stream (Gray and others, 2005; Fricker and others, 2007; Fricker and Scambos, 2009). This agrees with radar and borehole data that suggest variation in subglacial hydrology across ice-stream shear margins (Bentley and others, 1998; Vogel and others, 2005; Engelhardt and Kamb, 2013).

Models suggest that heat generated by shear in the ice-stream margins can lead to the development of temperate ice, which is ice at the local melting temperature that maintains some mechanical strength (Schoof, 2012; Suckale and others, 2014; Perol and Rice, 2015). Further work by deformation in the temperate ice produces melt water. Above a critical threshold, melt water drains to the bed and can be evacuated by subglacial hydrology (Perol and others, 2015).

Extensive antiplane shearing within the ice, i.e. variation in downstream velocity u_x over a (y, z) cross section, occurs at both the base of surging glaciers and across ice-stream shear margins. This antiplane shearing decreases the viscosity of ice, and here we examine how this affects R-channel closure. In an ice-stream shear margin, we schematically represent a subglacial hydrologic system with a single R-channel that we place near the transition between the locked, frozen till under the ridge and the slipping, failed till under the stream (Fig. 1a) (Perol and Rice, 2011; Suckale and others, 2014; Perol and others, 2015). The ice in this region is strongly sheared as it transitions from the plug flow in the centre of the stream to the much slower motion in the ridge. Under a mountain glacier, the antiplane shear arises from differential ice velocity with depth (Fig. 1b).

In this paper, we analyse the effects of including the existing antiplane shear on the creep closure of R-channels. We show that the amount of antiplane shear present in the ice can substantially increase the size of the R-channels or decrease the effective pressure, which can affect the duration of glacier surges and the location of ice-stream shear margins.

1.1. Classical R-channel theory

In an R-channel, liquid water flows turbulently through a conduit. The turbulent eddies dissipate heat at the wall and melt the ice, increasing the size of the channel. Simultaneously, the mass of ice surrounding the channel viscously creeps inward, closing the hole. In equilibrium, the creep closure of the ice is exactly balanced by the melting incurred by the turbulence.

For a single channel in a subglacial hydrologic system, Nye (1953) derives the creep closure velocity u_r , which in polar coordinates is written as

$$u_r(r) = -A \left(\frac{N}{n} \right)^n \frac{a^2}{r}, \quad (3)$$

where r is the distance from the centre of the channel, a is the radius of the channel and N is the effective pressure. The parameters A and n come from the ice rheology of a shear-

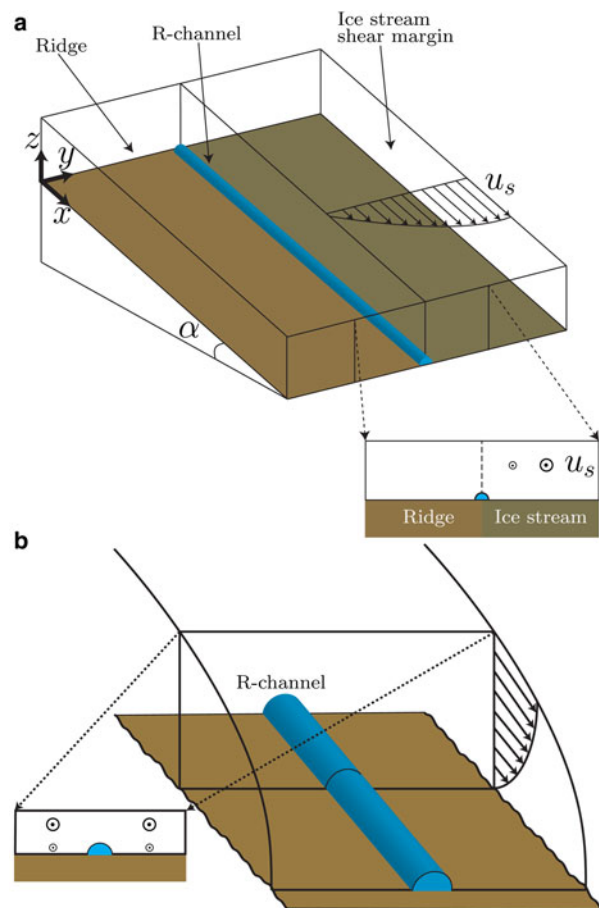


Fig. 1. Antiplane shear in ice streams and mountain glaciers: (a) Schematic representation of an R-channel in an ice stream shear margin. The ice flows at several hundred m a^{-1} in the stream with velocity u_s , while staying nearly stagnant in the ridge, which leads to an antiplane shear field around the R-channel. The inset shows a cross section of ice. Flow is out of the page (i.e. antiplane) and represented by dots enclosed by circles (arrow tips). The magnitude of the antiplane velocity is proportional to the size of the arrow tips. (Adapted from Schoof, 2004; Suckale and others, 2014; Perol and others, 2015.) (b) Schematic representation of an R-channel at the base of a mountain glacier. The velocity in the ice increases with height above the bed which leads to vertical shear around the R-channel.

thinning fluid with a power-law relationship between deviatoric stress and strain rates,

$$\dot{\epsilon}_E = A \tau_E^n, \quad (4)$$

where the subscript E indicates the second invariant of the tensor, A ($\text{s}^{-1} \text{Pa}^{-n}$) is the ice softness, and n is the rheological power, with $n > 1$ indicating shear thinning (Cuffey and Paterson, 2010). Depending on the creep mechanism and the stress magnitude, values from $n = 1$ to $n = 4$ are appropriate (Steinemann, 1954; Durham and others, 1997; Goldsby and Kohlstedt, 2001). We take $n = 3$ following Glen (1955), as is common in glaciology. We give representative values for parameters in Table 1. Nye (1953) compares the predictions from Eqn (3) with published data on the closure of tunnels in a variety of glaciers and finds that the closure expression works well in most cases, but fails when the stress state in the overlying ice is not exclusively hydrostatic (Haefeli, 1951; Glen, 1956; Weertman, 1972).

Table 1. Parameters similar to those from Siple Coast Ice Streams (Engelhardt and Kamb, 1997; Cuffey and Paterson, 2010; Suckale and others, 2014)

| | | | |
|---------------------|------------------------|----------------------------------|----------------------|
| ρ_{ice} | 910 | kg m ⁻³ | Ice density |
| ρ_{w} | 1000 | kg m ⁻³ | Water density |
| g | 9.8 | m s ⁻² | Gravity |
| \mathcal{L} | 333 500 | m ² s ⁻² | Latent heat per mass |
| n_{m} | 0.025 | s m ^{-(1/3)} | Manning coefficient |
| $\sin(\alpha)$ | 0.001 | – | Surface slope |
| A | 2.18×10^{-24} | s ⁻¹ Pa ⁻ⁿ | Ice softness |
| n | 3 | – | Rheological power |
| N | 5×10^5 | Pa | Effective pressure |

To model the flow of melt water, we treat the R-channel as a semicircular conduit for fully developed turbulence. The Manning–Strickler parameterisation for a turbulent flow in a rough-walled pipe is given as

$$Q = \frac{A_c R_h^{2/3} \sin^{1/2}(\alpha)}{n_m},$$

where n_m (s m^{-1/3}) is the Manning roughness coefficient, Q is the water discharge, $\sin(\alpha)$ is the slope driving flow (i.e. the bed slope in the idealised ice stream, or the local surface slope in the flat-bedded mountain glacier; Fig. 1; Table 1), A_c is the cross-sectional area, and R_h is the hydraulic radius, which is defined as $R_h \equiv A_c/P_r$ for the wetted perimeter P_r (Henderson, 1966; Clarke, 2003). For a semicircular channel, we follow Weertman (1972) and write the flow rate as a function of the channel diameter D as

$$Q = \frac{\pi D^{8/3} \sin^{1/2}(\alpha)}{2^{13/3} (1 + 2/\pi)^{2/3} n_m}. \quad (5)$$

In the R-channel analysis, the water and ice are assumed to be at the melting temperature (Röthlisberger, 1972). Thus, all of the energy generated by the turbulent flow goes into melting at the channel walls. In steady state, with symbols defined in Table 1, we can write (Weertman, 1972):

$$\frac{\pi}{2} \rho_{\text{ice}} \mathcal{L} D u_{\text{melt}} = \rho_{\text{w}} g \sin(\alpha) Q. \quad (6)$$

In equilibrium, the melt velocity u_{melt} has the same magnitude as the creep closure velocity, $u_{\text{cr}} = |u_r(r=a)|$ but in opposite direction. The diameter of the R-channel is found by inserting Q from Eqn (5) into Eqn (6) and solving for D , using the fact that u_{melt} is the same as u_{cr} . The closed-form solution for the diameter of an R-channel is

$$D = 4 \left(1 + \frac{2}{\pi}\right)^{2/5} \left(\frac{\rho_{\text{ice}} \mathcal{L}}{\rho_{\text{w}} g} \frac{u_{\text{cr}} n_m}{\sin^{3/2}(\alpha)}\right)^{3/5}. \quad (7)$$

Inserting the Nye solution, Eqn (3), we find that

$$D_{\text{Nye}} = \left(\frac{2^{7/3} (1 + 2/\pi)^{2/3} \rho_{\text{ice}} \mathcal{L}}{n^n \rho_{\text{w}} g} \frac{A N^n n_m}{\sin^{3/2}(\alpha)}\right)^{3/2}. \quad (8)$$

Superimposed antiplane motion softens the ice, which increases the creep closure velocity u_{cr} beyond that predicted by the Nye solution and, thereby, increases the channel diameter D for a given water pressure in the channel.

2. MODEL

We use the standard coordinate system in glaciology with z running from the bed to the surface, y across glacier, and x down glacier. The in-plane terms act in the y – z plane (e.g. σ_{rr} and $\sigma_{\theta r}$) and the antiplane terms act in the downstream or x -direction (e.g. σ_{rx} or $\sigma_{\theta x}$). Figure 2a corresponds to Figure 1a and relates the quarter circle domain to an R-channel in an idealized ice-stream shear margin. In the centre of the ice stream the flow velocity is u_s and in the ridge there is no flow. To impose antisymmetry about the z -axis, we translate the system to a reference frame by $-y\dot{\gamma}_{\text{far}} = u_s/2$. In this reference frame, the margin is stationary and the stream and the ridge are moving at $u_s/2$ and $-u_s/2$ respectively. The same setup for a mountain glacier is depicted in Figure 2b, where the coordinate system has been rotated 90° to convert the vertical shear in the ice column into lateral shear. Under this rotation, the model domains for the idealized ice-stream shear margin and the mountain glacier coincide and they are shown dimensionally and non-dimensionally in Figures 2c, d, respectively.

We model a single R-channel incised into the ice in an idealised ice-stream shear margin or mountain glacier. Several simplifications are made in this analysis. We consider a perfectly flat bed without protrusions, cavities or till deformation. For basal boundary conditions, we use stress-free conditions at the base of the ice stream and no slip conditions at the bed of the mountain glacier. We neglect connections to other subglacial drainage pathways outside the R-channel. Furthermore, we neglect sediment transport and erosion of the sediment beneath the R-channel, prohibiting the formation of Nye channels or canals. These simplifications allow us to focus on the effects of ice deformation on the closure of R-channels.

We treat the ice as a homogeneous fluid with a Glen's law rheology, i.e. Eqn (4). The effective stress and strain rates are given in polar coordinates as

$$\tau_E = \sqrt{\frac{1}{4}(\sigma_{rr} - \sigma_{\theta\theta})^2 + \sigma_{\theta r}^2 + \sigma_{rx}^2 + \sigma_{\theta x}^2}, \quad (9)$$

$$\dot{\epsilon}_E = \sqrt{\dot{\epsilon}_{rr}^2 + \dot{\epsilon}_{\theta r}^2 + \dot{\epsilon}_{rx}^2 + \dot{\epsilon}_{\theta x}^2}. \quad (10)$$

Relating the deviatoric stress and strain rates using Eqn (4), we write the strain rates in cylindrical polar coordinates as

$$\dot{\epsilon}_{rr} = \frac{\partial u_r}{\partial r} = \frac{1}{2} A \tau_E^{n-1} (\sigma_{rr} - \sigma_{\theta\theta}), \quad (11)$$

$$\dot{\epsilon}_{\theta\theta} = \frac{1}{r} \frac{\partial u_\theta}{\partial \theta} + \frac{u_r}{r} = \frac{1}{2} A \tau_E^{n-1} (\sigma_{\theta\theta} - \sigma_{rr}), \quad (12)$$

$$\dot{\epsilon}_{\theta r} = \frac{1}{2} \left(\frac{1}{r} \frac{\partial u_r}{\partial \theta} + \frac{\partial u_\theta}{\partial r} - \frac{u_\theta}{r}\right) = A \tau_E^{n-1} \sigma_{\theta r}, \quad (13)$$

$$\dot{\epsilon}_{rx} = \frac{1}{2} \frac{\partial u_x}{\partial r} = A \tau_E^{n-1} \sigma_{rx}, \quad (14)$$

$$\dot{\epsilon}_{\theta x} = \frac{1}{2r} \frac{\partial u_x}{\partial \theta} = A \tau_E^{n-1} \sigma_{\theta x}, \quad (15)$$

where $\dot{\epsilon}_{xx} = 0$ due to the plane strain constraint, and $\dot{\epsilon}_{rr} + \dot{\epsilon}_{\theta\theta} = 0$ due to the mass conservation.

Rather than using an infinite domain (e.g. Nye, 1953), we follow Evatt (2015) and consider a finite domain that runs from $r = \sqrt{y^2 + z^2} = a$ to $r = b$ as shown in Figure 2. We

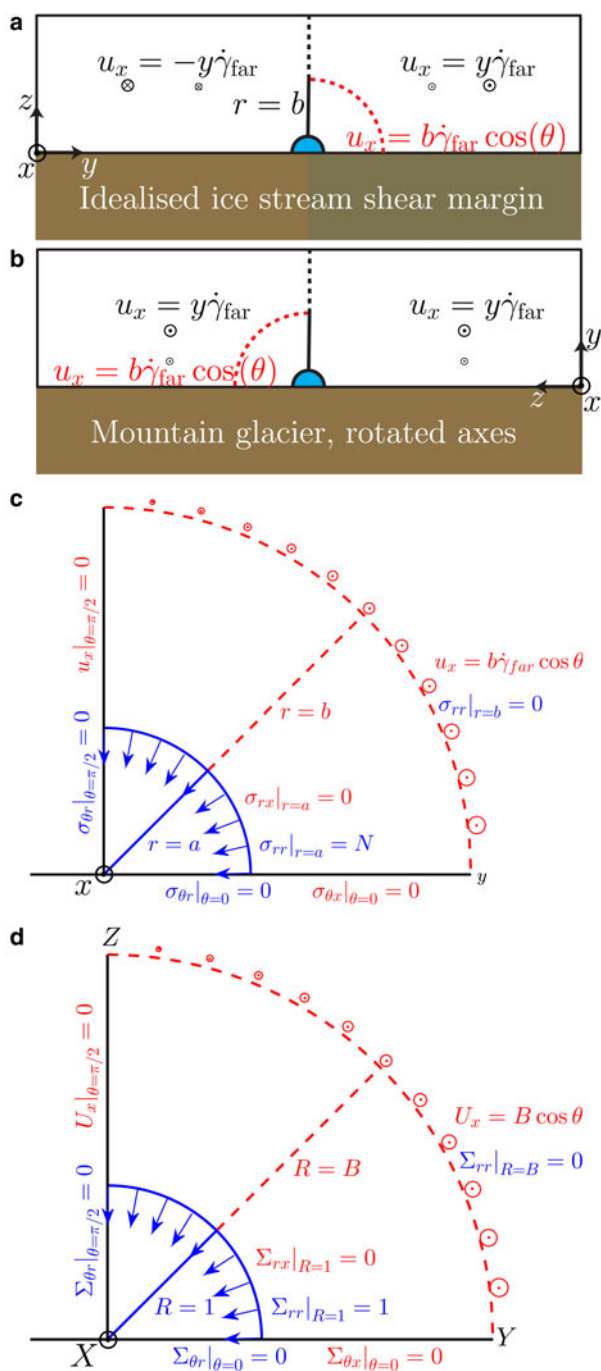


Fig. 2. Schematic representation for the quarter model domain shown in (a) an idealised ice stream shear margin and (b) a mountain glacier that has been rotated to translate vertical shear to lateral shear. These map to the physical space and boundary conditions for in-plane (blue) and antiplane (red) motion around a channel: (c) dimensionally and (d) non-dimensionally. In-plane motion occurs in the y - z plane and antiplane motion occurs in the x -direction. The coordinates are in a translating reference frame moving at $-\dot{\gamma}_{far}$, so that the system is antisymmetric about the z -axis.

do this for two reasons, firstly, it is more general and, secondly, the addition of antiplane shear can dominate in-plane motion in the far-field if the domain is too large. On the outer boundary of the finite domain, the normal stress is equal to the overburden (hydrostatic) pressure of the ice, $\rho_{ice}gH(1 - z/H)$, where H is the glacier thickness (Nye, 1953; Evatt, 2015). Assuming that $b/H \ll 1$ and therefore, that the overburden stress is nearly constant around the

domain, we write the constant compressive overburden stress as $\sigma_o = \rho_{ice}gH$. On the boundary of the channel, the normal stress is the water pressure inside the channel, p_w ($< \sigma_o$) following Spring and Hutter (1981). Due to incompressibility and the pressure independence of the assumed rheology, we can add to our stress field the uniform tensile stress $\sigma_o \delta_{ij}$, which has no effect on the flow field and removes any traction on the outer wall. This gives $\sigma_{rr}(r = a) = \sigma_o - p_w = N$ at the channel wall. Thus, the in-plane boundary conditions are

$$\sigma_{rr}(r = a) = \sigma_o - p_w = N, \quad \sigma_{rr}(r = b) = 0.$$

In the antiplane direction, the shear stress on the inner channel is zero. On the outer boundary, we impose an antiplane velocity u_x that varies linearly with distance $y = b \cos(\theta)$ to represent far-field shearing. In this way, we write the antiplane boundary conditions as

$$\sigma_{rx}(r = a) = 0, \quad u_x(r = b) = \dot{\gamma}_{far} b \cos(\theta).$$

In order to isolate the effects of antiplane shear generated by differential velocity within the ice, we apply the following boundary conditions along the base of the glacier or idealised ice-stream shear margin,

$$\sigma_{\theta r}(r; \theta = 0) = 0, \quad \sigma_{\theta x}(r; \theta = 0) = 0.$$

In a mountain glacier with rotated axes, these boundary conditions represent symmetry conditions (Fig. 2b). In the idealised ice-stream shear margin, however, these boundary conditions represent how the basal ice interacts with the till. We assume that the till deforms plastically (Kamb, 1991; Tulaczyk and others, 2000; Cuffey and Paterson, 2010) and $\sigma_{\theta x}(\theta = 0) \equiv \sigma_{zx}(z = 0) = \tau_b$, where τ_b is the basal shear stress supported by the till and less than or equal to the plastic yield stress of the till τ_y . If the basal shear stress τ_b is small compared with a characteristic antiplane shear stress within the ice τ_{far} , then the assumption $\sigma_{\theta x}(r; \theta = 0) \approx 0$ is well justified (Schoof, 2012). In recent numerical simulations, Perol and others (2015) find a basal shear stress of $\tau_b \approx 60 - 75$ kPa near an R-channel in an ice-stream shear margin. If we estimate the characteristic antiplane shear stress as $\tau_{far} = (\dot{\gamma}_{far}/2A)^{1/n} \approx 75$ kPa, using $\dot{\gamma}_{far} = 2 \times 10^{-9} \text{ s}^{-1}$ and $A = 2.18 \times 10^{-24} \text{ Pa}^{-n} \text{ s}^{-1}$ (cf. Fig. 3; Table 1), we find that τ_{far} and σ_{zx} from the simulations by Perol and others (2015) are of similar magnitude. Thus, near the channel $\sigma_{\theta x}(r; \theta = 0) \approx 0$ is potentially a poor approximation to the subglacial hydrology influenced basal boundary conditions prescribed by Perol and others (2015). Furthermore, including in-plane traction along the ice/till interface, i.e. $\sigma_{\theta r}(r; \theta = 0) = \tau_b$, would inhibit channel closure at the base (Weertman, 1972). It is likely all the same that this is a small effect due to the small channel closure velocities. Nevertheless, our goal is to isolate the effects of antiplane shear within the ice and therefore, we neglect antiplane and in-plane basal shear (Hutter and Olinloyo, 1980; Barcilon and Macayeal, 1993; Haseloff and others, 2015). These channels can also be thought of as fully circular englacial channels, as the conditions $\sigma_{\theta x}(r; \theta = 0) = 0$ and $\sigma_{\theta r}(r; \theta = 0) = 0$ enforce symmetry across the y -axis.

Along the vertical axis of the quarter circle domain we apply the boundary conditions:

$$\sigma_{\theta r}(r; \theta = \pi/2) = 0, \quad u_x(r; \theta = \pi/2) = 0.$$

These represent symmetry and antisymmetry conditions and are consistent with the boundary conditions applied at the outer edge. For the mountain glacier with rotated axes, the condition $u_x = 0$ amounts to a no slip boundary condition at the base, which is an approximation unless the base is frozen to the bed or pore pressure is depressed in the basal till (Hindmarsh, 2004; Cuffey and Paterson, 2010).

Scaling all lengths by the channel radius a , we have $r = aR$ and the dimensionless outer radius $B = b/a$, which defines the domain size. We scale the antiplane shear strain rate by $\dot{\gamma}_{\text{far}}$ and the in-plane components of strain rate by AN^n , which is the dimensional scaling of the Nye strain rate, so that $\dot{\epsilon}_{rr} = AN^n \dot{E}_{rr}$. A consequence of this scaling is that the strain rates will not necessarily be close to unity: at the edge of the channel $\dot{E}_{rr} = n^{-n}$, which is 1/27 for $n = 3$. We can non-dimensionalise the effective strain rate in the same way as the in-plane strain rates, which gives

$$\dot{E}_E = \sqrt{\dot{E}_{rr}^2 + \dot{E}_{\theta r}^2 + S^2(\dot{E}_{rx}^2 + \dot{E}_{\theta x}^2)}, \quad (16)$$

where S is the strain rate ratio of antiplane to in-plane strain rates

$$S = \frac{\dot{\gamma}_{\text{far}}}{AN^n}. \quad (17a)$$

This ratio represents the importance of the superimposed antiplane shear strain rate $\dot{\gamma}_{\text{far}}$, as compared with a characteristic in-plane strain rate AN^n .

The strain rate ratio S can also be written as:

$$S = n^{-n} \left(\frac{\dot{\gamma}_{\text{far}}}{\dot{\epsilon}_{\theta\theta}^{\text{Nye}}} \right), \quad (17b)$$

$$= 2 \left(\frac{\tau_{\text{far}}}{N} \right)^n, \quad (17c)$$

where we use

$$\dot{\epsilon}_{\theta\theta}^{\text{Nye}} = A \left(\frac{N}{n} \right)^n \quad \text{and} \quad \tau_{\text{far}} = \left(\frac{\dot{\gamma}_{\text{far}}}{2A} \right)^{1/n}.$$

Thus, S represents the importance of the antiplane strain rate imposed on the outer edge of the domain to the in-plane creep closure of the channel.

Since the stress driving creep closure at the edge of the channel scales with N , we non-dimensionalise the in-plane stresses so that $\sigma_{rr} = N\Sigma_{rr}$. Following the above convention for the antiplane strain rates, we scale antiplane stresses by SN so that $\sigma_{rx} = SN\Sigma_{rx}$. We now write the effective stress as $\tau_E = NT_E$, where

$$T_E = \sqrt{\frac{1}{4}(\Sigma_{rr} - \Sigma_{\theta\theta})^2 + \Sigma_{\theta r}^2 + S^2(\Sigma_{rx}^2 + \Sigma_{\theta x}^2)}. \quad (18)$$

The velocities scale as the strain rates multiplied by the channel radius so that

$$u_r = AaN^n U_r \quad \text{and} \quad u_x = AaN^n S U_x. \quad (19)$$

The equations for mass and momentum conservation now

become

$$\frac{1}{R} \frac{\partial}{\partial R} (R\Sigma_{rr}) + \frac{1}{R} \frac{\partial \Sigma_{\theta r}}{\partial \theta} - \frac{\Sigma_{\theta\theta}}{R} = 0, \quad (20)$$

$$\frac{1}{R} \frac{\partial}{\partial R} (R\Sigma_{\theta r}) + \frac{1}{R} \frac{\partial \Sigma_{\theta\theta}}{\partial \theta} + \frac{\Sigma_{\theta r}}{R} = 0, \quad (21)$$

$$\frac{1}{R} \frac{\partial}{\partial R} (R\Sigma_{rx}) + \frac{1}{R} \frac{\partial \Sigma_{\theta x}}{\partial \theta} = 0, \quad (22)$$

$$\dot{E}_{rr} + \dot{E}_{\theta\theta} = \frac{dU_r}{dR} + \frac{U_r}{R} + \frac{1}{R} \frac{\partial U_\theta}{\partial \theta} = 0. \quad (23)$$

The boundary conditions, in non-dimensional form (Fig. 2d), are then

$$\Sigma_{rr}(R = 1) = 1, \quad \Sigma_{rr}(R = B) = 0,$$

$$\Sigma_{rx}(R = 1) = 0, \quad U_x(R = B) = B \cos(\theta),$$

$$\Sigma_{\theta r}(R; \theta = 0) = 0, \quad \Sigma_{\theta x}(R; \theta = 0) = 0,$$

$$\Sigma_{\theta r}(R; \theta = \pi/2) = 0, \quad U_x(R; \theta = \pi/2) = 0.$$

2.1. Reasonable strain rate ratio values

Here we estimate the size of the antiplane strain rate $\dot{\gamma}_{\text{far}}$ using data from the the Worthington Glacier, Alaska (Harper and others, 2001), which is shown in Figure 3a, and the Upper Whillans Ice Stream shear margin surface velocity data shown in Figure 3b (Echelmeyer and Harrison, 1999; Truffer and Echelmeyer, 2003, 2005). These data give the estimates of $\dot{\gamma}_{\text{far}} = 2 \times 10^{-8} \text{ s}^{-1}$ for mountain glaciers and $\dot{\gamma}_{\text{far}} = 4 \times 10^{-9} \text{ s}^{-1}$ for ice-stream shear margins. We then combine the value for the antiplane strain rate $\dot{\gamma}_{\text{far}}$ with a representative value for the effective pressure N to compute the strain rate ratio $S = \dot{\gamma}_{\text{far}}/AN^n$. We also note that the actual value can vary quite significantly, leading to changes in the value of S . The ranges of S we find for reasonable parameter values are $S \sim 10^{-4}$ – 10^{-2} for mountain glaciers and $S \sim 10^{-3}$ – 10^{-1} for ice-stream shear margins. These ranges serve as guidelines for what values of S are relevant to channels in antiplane shear, as in how channel size and shape might vary with S .

2.1.1. Mountain glaciers

We estimate the strain rate ratio S as

$$S \sim \frac{u}{AhN^n},$$

where u and h are the velocity difference and height of basal shear (Fig. 3a). For example, data from Harper and others (2001) and Bartholomaeus and others (2011) as well as Cuffey and Paterson (2010), suggest the estimates

$$u \approx 21 \text{ m a}^{-1}, \quad A \approx 2.4 \times 10^{-24} \text{ s}^{-1} \text{ Pa}^{-n},$$

$$h \approx 33 \text{ m} \quad \text{and} \quad N \approx 1.35 \times 10^6 \text{ Pa}.$$

The effective pressure is similar to the values reported by Kavanaugh and Clarke (2000), Flowers and Clarke (2002b) and Schoof and others (2014). Combining these estimates

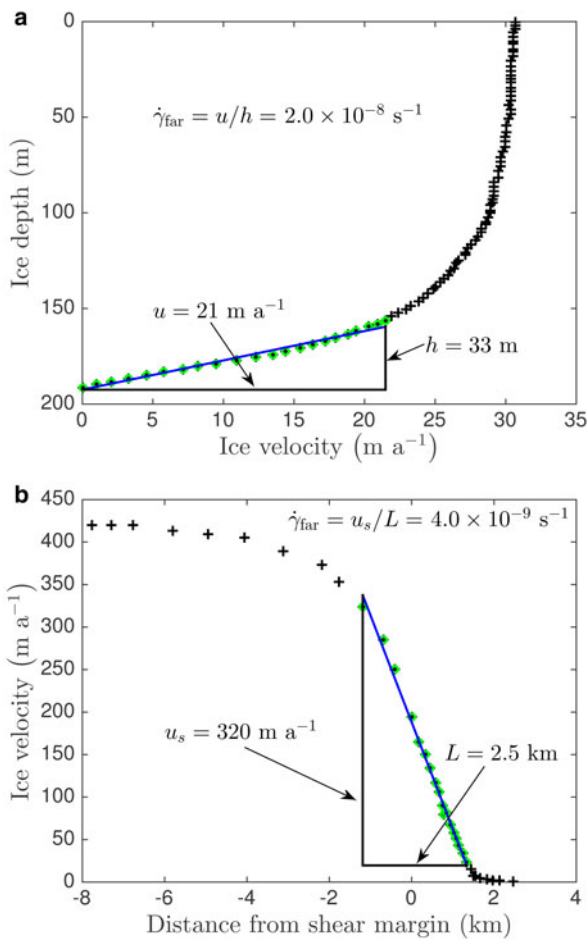


Fig. 3. Velocity data for computing the magnitude of the antiplane strain rate $\dot{\gamma}_{\text{far}}$: (a) Ice velocity with depth for Worthington Glacier, Alaska from Harper and others (2001). (b) Ice stream shear margin surface velocity data between stations S17 and UpB on the Upper Whillans Ice Stream, Siple Coast, West Antarctica from January 1994 to January 1995 (Echelmeyer and Harrison, 1999; Truffer and Echelmeyer, 2003, 2005). The green circles indicate the portion of the shear zone used to calculate the slope shown in the figure.

we find a strain rate ratio of

$$S \approx 10^{-3}.$$

By varying the parameters slightly we find a representative range of $S \sim 10^{-4} - 10^{-2}$.

2.1.2. Ice-stream shear margins

The scaling for the strain rate ratio in ice-stream shear margins is similar to the scaling for mountain glaciers except that the length scale L is now the width of the shear margin (Fig. 3b), so that

$$S \sim \frac{u_s}{ALN^n}.$$

The velocity profile in the ice stream and its shear margin are approximately uniform with depth allowing us to use the measured surface velocity u_s to describe the flow at the base (Kamb, 2001). Using the data from Echelmeyer and Harrison (1999), Joughin and Tulaczyk (2002), as well as Cuffey and Paterson (2010), we choose the parameters

$$u_s \approx 320 \text{ m a}^{-1}, A \approx 2.18 \times 10^{-24} \text{ s}^{-1} \text{ Pa}^{-n}, \\ L \approx 2500 \text{ m and } N \approx 5 \times 10^5 \text{ Pa}.$$

Since R-channels operate at lower water pressure (larger effective pressure) than water flow through linked cavities or sediments, the value for the effective pressure used here is larger than found by Blankenship and others (1987) for the water-saturated subglacial till under Ice Stream B (Whillans Ice Stream). Moreover, the water pressure beneath the ice streams is still closer to the overburden pressure than in mountain glaciers (Engelhardt and Kamb, 1997, 1998; Tulaczyk and others, 2001). These parameters lead to strain rate ratio of about

$$S \approx 10^{-2},$$

which varies in the range $S \sim 10^{-3} - 10^{-1}$ for slightly different parameter values.

3. ANALYSIS

The estimates for S from mountain glaciers and ice streams show that it is a small quantity. In this limit of small antiplane shear, we are able to derive a closed-form solution for the antiplane velocity, which allows us to benchmark the combined in-plane and antiplane finite element code that is used for later calculations. After examining the small S limit, we then turn to the opposite limit, when antiplane motion dominates, and find a scaling for the creep closure as a function of S . The reader who is primarily interested in how the R-channel diameter scales with S and non-circular R-channels can skip to the next section.

For our numerical solutions, we use the existing numerical finite-element method (FEM) package ABAQUS (Dassault Systèmes, 2012). To model the fully coupled problems, where the ice viscosity is a function of both the in-plane and the antiplane components, we construct a single-element thick, three-dimensional FEM model constrained to deform by a combination of plane strain and antiplane strain. We couple the displacements of the nodes on opposite faces to ensure that the model maintains a state of combined antiplane and plane strain. We generate the FEM using isoparametric elements with significant refinement near the channel boundary. We compare numerical solutions to the known in-plane Nye solution without antiplane shearing and find a nodal error of $<0.8\%$.

3.1. Small antiplane velocity benchmark

Here, we show that when S is very small we can derive an analytical solution for the antiplane velocity. The reason for considering this limit is that when the applied antiplane shear is sufficiently small, the in-plane motion dominates throughout the domain and sets the viscosity of the ice. Thus, the creep closure of the R-channel is given by the Nye solution. Evatt (2015) gives a derivation for the finite domain Nye solution, which in the dimensionless variables used here is given as

$$U_r = -\frac{n^{-n}}{R} \frac{B^2}{(B^{2/n} - 1)^n}. \quad (24)$$

In this limit, the effective deviatoric stress is only a function of R and given as

$$T_E = \frac{1}{2} (\Sigma_{rr} - \Sigma_{\theta\theta}) = \frac{1}{nR^{2/n}} \left(1 - \frac{1}{B^{2/n}} \right)^{-1}.$$

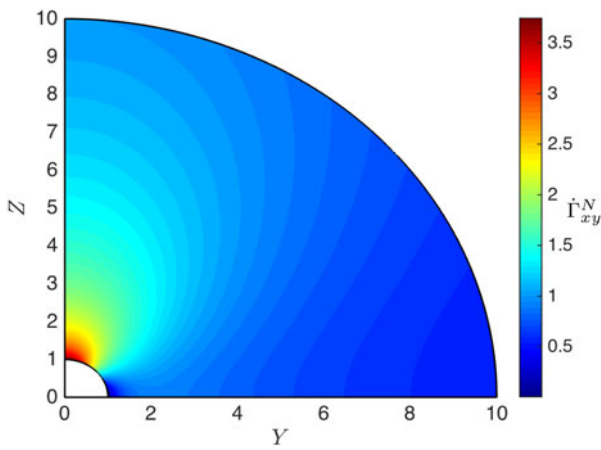


Fig. 4. Horizontal antiplane strain rate $\partial U_x/\partial Y$ for $S \ll 1$, small antiplane perturbation of in-plane flow field: ABAQUS numerical solution $\dot{\Gamma}_{xy}^N$ to the full problem with $S = 10^{-4}$. The maximum value of horizontal strain rate is $<0.1\%$ from the analytical solution of 3.7472 as calculated from the derivative of Eqn (26) and is located on the top of the channel.

Using Eqns (14) and (15), we can insert the effective stress into the in-plane force balance, Eqn (20), and find

$$R^{(2/n)-1} \frac{\partial}{\partial R} \left(R^{3-(2/n)} \frac{\partial U_x}{\partial R} \right) + \frac{\partial^2 U_x}{\partial \theta^2} = 0. \tag{25}$$

This is an equidimensional, linear equation for the antiplane velocity u_x . The antiplane boundary conditions are

$$\left. \frac{\partial U_x}{\partial \theta} \right|_{\theta=0} = 0, \left. \frac{\partial U_x}{\partial R} \right|_{R=1} = 0 \quad \text{and} \quad U_x(R = B) = B \cos(\theta).$$

A method to solve Eqn (25) subject to these boundary conditions is described in Appendix A. The solution for the antiplane velocity u_x is

$$U_x = B \frac{(R^{\lambda_+/\lambda_+} - R^{\lambda_-/\lambda_-})}{(B^{\lambda_+/\lambda_+} - B^{\lambda_-/\lambda_-})} \cos(\theta), \tag{26}$$

where λ_+ and λ_- are positive and negative solutions to the characteristic polynomial, Eqn (A1) for $k = 1$. Equation (26) also shows that points at the edge of the channel displace in the antiplane direction as if the interior underwent a homogeneous deformation rate and therefore, similar to an Eshelby (1957) inclusion in a composite solid. Figure 4 shows the numerical strain rate $\dot{\Gamma}_{xy}^N$ computed from the full ABAQUS simulation with $S = 10^{-4}$. The error between $\dot{\Gamma}_{xy}^N$ and the derivative of Eqn (26), $\partial U_x/\partial Y$ is $<0.1\%$ and serves as a good benchmark for the ABAQUS simulations.

3.2. Region of validity

We now consider under what conditions the analytical solution for the antiplane velocity is valid. From the Nye solution, Eqn (24), we can see that the in-plane velocity decays as $1/R$. The antiplane velocity, however, is largest along the outer edge. Thus, for the perturbation solution to be valid throughout the domain, we require that the ratio of antiplane shear strain rate to the minimum in-plane strain rate is small, i.e.

$$\frac{\dot{\gamma}_{\text{far}}}{\dot{\epsilon}_{rr}(R = B)} = n^n S (B^{2/n} - 1)^n \ll 1.$$

We can rearrange the right-hand side to find the critical non-dimensional radius

$$B_{\text{cr}} = \left(1 + \frac{1}{nS^{1/n}} \right)^{n/2}. \tag{27}$$

Thus, the outer radius must satisfy the inequality $B \ll B_{\text{cr}}$ in order for the entire domain to be dominated by in-plane creep closure. This condition states that the domain size must decrease as S increases. For $S = 10^{-3}$ and $n = 3$, we have that $B_{\text{cr}} = 10$ and, thus for $B = 10$, this inequality is violated as S approaches 10^{-3} but not unity as one might initially expect.

If the size of the domain is much larger than B_{cr} , the perturbation solution is no longer valid near the boundary and there is a transition to a region that is antiplane dominated (Weertman, 1972). The small S scaling of Eqn (27) predicts that the transition will occur at a radius $R \sim 1/\sqrt{S}$, as this is when $\dot{\epsilon}_{rr} \sim S$. Close to the channel, the dominant flow of ice is inward creep closure of the channel. In the far field, ice predominantly flows downstream. The transition radius, $R \sim 1/\sqrt{S}$, represents the crossover between the inward creep closure dominated flow and the antiplane flow downstream.

3.3. Limit of large antiplane velocity

Here we consider very large values of S , when antiplane shear strain rate strongly dominates the in-plane strain rate. In this limit, the non-dimensional effective stress and strain rate, from Eqns (9) and (10), reduce to

$$\tau_E = S \sqrt{\Sigma_{rx}^2 + \Sigma_{\theta x}^2} \quad \text{and} \quad \dot{\epsilon}_E = S \sqrt{\dot{\epsilon}_{rx}^2 + \dot{\epsilon}_{\theta x}^2}. \tag{28}$$

Thus, the effective viscosity of the ice is set by the antiplane motion. In this regime, the non-linearity of the equations in the in-plane direction disappears and the channel will close like a Newtonian ($n = 1$) fluid with a spatially variable viscosity, much like the observations of Haefeli (1951) and Glen (1956). Here we seek to determine how the creep closure velocity U_r depends on S .

To start, we use quantities that are averaged over $\theta \in [0, \pi]$ and consider deviations from axisymmetric creep closure in a later section. Mass conservation can then be written as

$$\frac{\partial \bar{U}_r}{\partial R} + \frac{\bar{U}_r}{R} = 0,$$

where any U_θ dependence integrates out, and we can write the solution \bar{U}_r in the form,

$$\bar{U}_r = -\frac{C}{R}. \tag{29}$$

Now in the large S limit, the in-plane rheology is given as

$$\dot{\epsilon}_{rr} = \frac{1}{2} S^{(n-1)/n} \left(\dot{\epsilon}_{rx}^2 + \dot{\epsilon}_{\theta x}^2 \right)^{(n-1)/(2n)} (\Sigma_{rr} - \Sigma_{\theta\theta}). \tag{30}$$

Along the channel, the radial stress and hoop stress scale as

$$\Sigma_{rr} - \Sigma_{\theta\theta} \sim f(n, B)$$

from the boundary conditions, where $\Sigma_{rr} = 1$ and $\Sigma_{\theta\theta}$ is

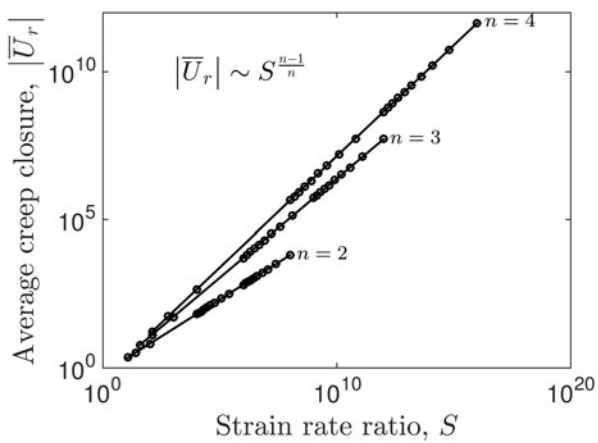


Fig. 5. Large S scaling for the average creep closure $|\bar{U}_r|$ at $R = 1$. Black circles are ABAQUS simulation results (linear spacing in S) and black lines follow scaling with a best-fit coefficient of proportionality. The outer radius for these simulations is $B = 10$.

independent of S and an unknown function of n and B . The radial antiplane strain rate \dot{E}_{rx} along the hole is zero and therefore we are left with

$$\bar{E}_{rr} \sim S^{n-1/n} \dot{E}_{\theta x}^{n-1/n} f(n, B).$$

The average in-plane strain rate scales with the in-plane velocity as

$$\bar{E}_{rr} \sim -\bar{E}_{\theta\theta} \sim -\frac{\bar{U}_r}{R},$$

and inserting the strain rate scaling at $R = 1$ gives

$$|\bar{U}_r| \sim S^{(n-1)/n},$$

which can be seen in Figure 5 for three different values of n and $B = 10$.

4. R-CHANNEL DIAMETER WITH S

In the previous two sections, we examined the creep closure velocity in the limits of small and large antiplane strain rate. Here we show the influence of antiplane shear on the size of R-channels. For the small antiplane shear case, e.g. $S \ll 1$, there is no change to the standard Röthlisberger analysis and we can insert the parameters from Table 1 into Eqn (8) and find that

$$D_{\text{Nye}} = \left(\frac{2^{7/3} (1 + 2/\pi)^{2/3} \rho_{\text{ice}} \mathcal{L} AN^n n_m}{n^n \rho_w g \sin^{3/2}(\alpha)} \right)^{3/2} \approx 2.3 \text{ m}.$$

This is consistent with Vogel and others (2005), who show flowing water with a depth of 1.6 m at the base of the dormant Kamb ice-stream shear margin.

For arbitrary S , we turn to numerical simulations to determine the average creep closure velocity \bar{u}_{cr} as a function of the applied antiplane strain rate $\dot{\gamma}_{\text{far}}$ and a fixed effective pressure N . Figure 6 shows that for $S \leq 10^{-3}$, the Nye solution holds and the predicted channel size is exactly that found above. As S increases, it leaves the small perturbation range and we find that for $S \sim 10^{-2}$, the diameter roughly

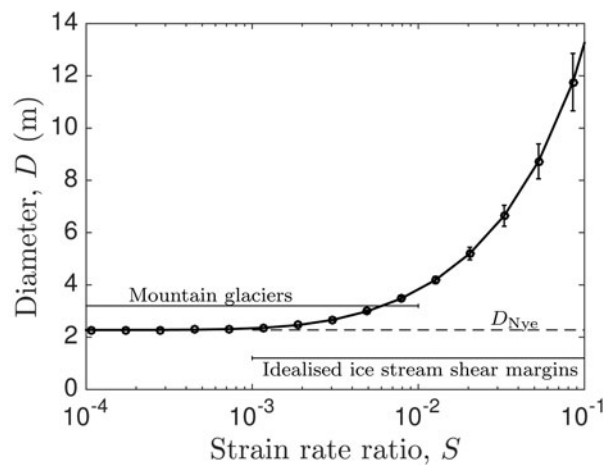


Fig. 6. R-channel diameter as a function of the antiplane to in-plane strain rate ratio S . Representative ranges of S for ice streams and mountain glaciers are based estimates from data (Echelmeyer and Harrison, 1999; Harper and others, 2001; Truffer and Echelmeyer, 2005). Error bars denote RMS deviations from axisymmetry.

doubles in size. For very large S , we can use the scaling from the last section to show that the diameter of the channel should scale as $D \sim S^{3(n-1)/(2n)}$. As S increases the R-channel size increases, which can be seen from Eqn (7): for a constant N , if \bar{u}_{cr} increases then D must also increase. A larger diameter also implies larger discharge Q and therefore, sufficient available water is required for the channel shape to increase at constant effective pressure.

If the channel pressure is allowed to vary, our results indicate that adding in antiplane shear allows channels at a given diameter (or flow rate) to operate at higher water pressures (lower effective pressure). For an R-channel with a fixed diameter, the flow rate through the channel is fixed by Eqn (5), and the creep closure rate of the channel is then fixed by Eqn (6). Our results in Figure 5 show that the creep closure velocity increases with $S = \dot{\gamma}_{\text{far}}/(AN^n)$. Thus, to maintain a fixed creep closure rate with a fixed far-field strain rate $\dot{\gamma}_{\text{far}}$, the channel pressure must increase, leading to a lower effective pressure and a reduction in the strength of the bed.

5. DISCUSSION

Here we discuss implications of increasing antiplane shear around R-channels to subglacial hydrology and extend our analysis to determine non-circular R-channel shapes. In Figure 6, we show the average R-channel diameter as a function of the strain rate ratio S , assuming a semicircular channel. Our numerical simulations do, however, allow for analysis of the expected shape and how the deviations from circular vary with applied antiplane shear. After discussing non-circular R-channels, we describe how our results for the diameter of an R-channel in regions of antiplane shear might influence subglacial hydrology and glacier sliding. We discuss the implications of these results to surging glaciers and describe how the transition between channelised drainage and linked-cavity systems may be facilitated by including shear in the R-channel analysis. Finally, we examine the relationship between the outer boundary of the domain and the applied antiplane shear and its implications for subglacial hydrology.

5.1. Non-circular R-channels

There is a small but growing literature on non-circular R-channels. Hooke and others (1990) consider channel cross sections given by the space between the arc of a circle and its chord and find better agreement with water pressure data from Austdalsbreen and Storglaciären than standard semicircular R-channels. Fowler and Ng (1996) model low, broad canals in sediments during jökulhlaups. In their model, the height of the channel is governed by the creep closure of ice and the width of the channel is determined by erosion of the sediments. This method provides more reasonable values for the Manning roughness coefficient and yields an improved simulation of the 1972 Grímsvötn jökulhlaup. Cutler (1998) uses a finite element model to determine the seasonal evolution of an R-channel cross section and examine the effects of variable water input. He finds that all channels tend toward low, broad shapes. Furthermore, for two channels with equivalent areas, the channel with a lower width-to-height ratio (i.e. more circular) will expand faster, stealing water from neighbouring channels. More recently, Dallaston and Hewitt (2014) study the stability of R-channels under coupled interfacial melting and creep closure. They show that circular channels under axisymmetric in-plane loading with a constant melt rate are unstable to linear perturbations for both shear-thinning and Newtonian viscosities. Moreover, they show that this instability can be stabilised by the addition of a uniform heat source that diffuses to the free boundary of the channel.

We complement these studies by examining how antiplane shear modifies initially circular channels. To analyse the effect of shear on the shape of the channel, we break the creep closure into an average and fluctuating component, i.e.

$$u_r = \bar{u}_{cr} + u'_r.$$

Our previous analysis neglected u'_r/\bar{u}_{cr} as a very small quantity. This assumption is reasonable because the maximum value of u'_r/\bar{u}_{cr} for $S = 10^{-1}$ is 0.1. However, we wish to look at channels that deviate from circular. In keeping with the idea that $u'_r/\bar{u}_{cr} \ll 1$, we ignore small variations in diameter and derive Eqn (7) identically as before. We then insert u_r in the place of \bar{u}_{cr} in Eqn (7), which gives approximately

$$D = 4 \left(1 + \frac{2}{\pi}\right)^{2/5} \left(\frac{\rho_{ice} \mathcal{L}}{\rho_w g} \frac{\bar{u}_{cr} n_m}{\sin^{3/2}(\alpha)}\right)^{3/5} \left[1 + \frac{3}{5} \frac{u'_r}{\bar{u}_{cr}}\right]. \quad (31)$$

Inserting u'_r , which is dependent on θ , from the simulations into Eqn (31), we plot the cross section of the channels for three values of S in Figure 7. We can see that the deviations from circular are not noticeable at $S = 2 \times 10^{-3}$ and it is not until $S \gtrsim 10^{-2}$ that the deviations become significant. The extent to which the channels deviate from circular are plotted as error bars in Figure 6.

The channel shapes predicted by our simulations indicate that when the superimposed antiplane strain rate increases, the creep closure velocity increases on the top of the channel (i.e. along the z -axis of Fig. 2) and decreases on the sides (along y -axis) relative to the average creep closure velocity \bar{u}_{cr} . This makes sense, in light of Figure 4, where the antiplane strain rate concentrates on the top of the channel and since the viscosity is lower, the channel

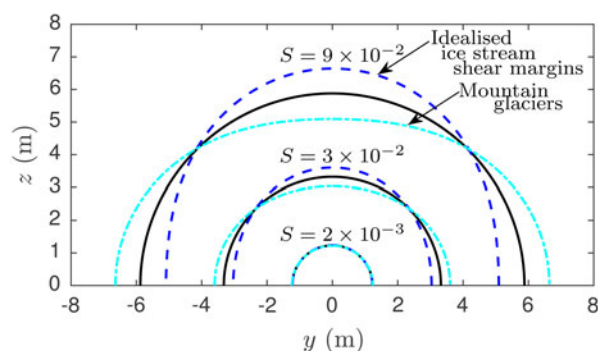


Fig. 7. Numerical prediction for the shape of R-channels as a function of S : The vertical shear present in mountain glaciers leads to short, broad channels that are wider than tall (cyan dot dashed curves) and the lateral shear in idealised ice stream shear margins leads to channels that are taller than wide (blue dashed curves). The azimuthally averaged velocity results in semicircular channels (black solid curves).

closes faster locally. Thus, using a melt rate proportional to the creep closure velocity (i.e. steady-state non-uniform melting), circular channels deform and melt into channels that are taller than they are wide. In mountain glaciers under vertical antiplane shear our simulations predict channels that are wider than tall, which is in agreement with the observations (e.g. Fountain, 1993; Hock and Hooke, 1993; Fountain and Walder, 1998). In idealised ice-stream shear margins, the antiplane shear straining is along the axis of the channel and our simulations indicate that channels that are taller than wide might form.

5.2. Implications for subglacial hydrology

In models of subglacial hydrology, the downstream ice velocity typically is ignored in the creep closure of the R-channels. Here we find that for low ice flow velocities, it is reasonable to neglect the effect of shear on the channel size, but in regions of high-velocity gradients, the channel size can increase significantly for a fixed pressure difference. This equivalently implies that for a fixed volume flux of water (or equivalently R-channel diameter), the channel will operate at a higher water pressure (lower effective pressure). Therefore, decreasing the effective pressure by accounting for antiplane shear, can increase the basal sliding velocity for a constant basal shear stress.

By including the feedback between antiplane shear and effective pressure, the transition between channelised and distributed drainage occurs at a lower effective pressure and a switch between the two styles of drainage may be facilitated. For hydrologically controlled surging glaciers, systems of channels can coexist with distributed drainage networks (Fowler, 1987, 1989, 2011). If the flux of water in the system increases slightly, then the effective pressure in the distributed network increases but decreases in the channels. The channelised portion of the hydrologic system can be unstable. As the flow rate increases, if the effective pressure in the channels decreases more than the distributed drainage effective pressure, then the drainage through channels can shut off. This mechanism leaves only a distributed drainage network that favours sliding. Traditionally, the basal sliding velocity u_b is related to the effective pressure in the distributed network via Eqn (1), and therefore, there

is a transition from channels to distributed drainage when $S_\Lambda = u_b/(AHN^n)$ reaches a critical value. This relationship can then be inserted into Eqn (1) to give a multivalued sliding law, where one branch is consistent with surging behaviour (Clarke and others, 1984; Fowler, 1989; Sayag and Tziperman, 2009). If we include the S dependence in the R-channel analysis, the effective pressure in the channels would decrease with increasing S , facilitating the transition to a distributed network for a fixed critical S_Λ .

5.3. Transitions in rheology around R-channels

Spatial transitions in ice rheology can also have profound implications for subglacial hydrology. For a small applied antiplane strain rate, we derive a condition on the outer radius, which ensures that the effective viscosity is dominated by in-plane creep closure throughout the domain. The inequality that the outer radius must satisfy sets an upper limit on the outer radius of the domain B based on S , i.e. Eqn (27). If the outer radius is larger than B_{cr} , a transition to an antiplane-dominated region occurs. Weertman (1972) also finds a transition from an in-plane-dominated to antiplane-dominated region and shows that the in-plane-dominated region deforms as a power-law fluid with $n = 3$ and the antiplane-dominated region in the far-field deforms as a Newtonian fluid with $n = 1$. In the case of a channel beneath an idealised glacier that slides over a flatbed without protrusions, a transition in ice rheology has implications for subglacial hydrology. The water pressure gradient, which drives the flow of water at the base of the glacier and is the derivative of the hoop stress, changes sign for different values of the rheological power n . Weertman finds that for $n > 2$ ($n < 2$) water is driven into (out of) an R-channel. Thus, in the antiplane-dominated limit water is driven out of the channel and driven into the channel in the in-plane-dominated limit. Weertman finds that the distance to this transition radius scales as $R \sim 1/S_\tau^{n/2}$, where $S_\tau = \tau/N$ and τ is the antiplane basal shear stress. For $S_\tau = 1/30$, Weertman shows that R-channels can pull water from a distance of $r \sim 160a$. Here we find that the transition scales as $R \sim 1/\sqrt{S}$, which leads to the prediction that R-channels can only pull water from a distance of about $r \sim a/\sqrt{S} \approx 6a$ or three channel diameters for $S \approx 1/30$. Thus, our analysis predicts a tighter spacing of channels as compared with Weertman's results, which has implications for the dendritic structure of channels.

6. CONCLUSION

Using an idealised, theoretical framework, we analyse how antiplane shear can affect the in-plane creep closure of an R-channel. For a small perturbation in $S = \dot{\gamma}_{far}/(AN^n)$, the effective viscosity is independent of the antiplane motion at leading order and therefore, there is no effect on the creep closure of the R-channel. With the ice viscosity set by the in-plane Nye solution, we find an analytical solution for the antiplane velocity u_x . In the finite domain, the outer radius must satisfy an inequality or else there is a transition to an antiplane-dominated region near the edge of the domain. For very large S , the entire domain is antiplane dominant and we derive a scaling for the average creep closure as a function of S . Combining the insight from both regimes, our analysis shows that small amounts of antiplane shear ($S \ll 10^{-3}$) have no effect on the R-channel size, but even

moderate amounts ($S \sim 10^{-2}$) of antiplane shear can double the average diameter of the R-channel. The dependence on antiplane shear in the R-channel analysis can affect glacier sliding by modulating the water pressure and therefore, the transition between channelised and distributed systems in surging glaciers. We also analyse the shape of R-channels under applied antiplane shear. We find agreement with observations of channels that are wider than tall beneath mountain glaciers as well as predict channels that are taller than wide could potentially form near zones of lateral antiplane shear.

Our ice-stream shear margin and mountain glacier schematics are simplified in order to understand the effects of antiplane shear around a single R-channel bounded by simple ice flow. Ice thermomechanics and drainage are more diffuse than our model implies and a transition in rheology will likely be smoother in space. Furthermore, in our model we neglect the mechanics of unsaturated till near an R-channel (Ng, 2000), the interaction between channelised and distributed drainage systems (Hewitt, 2011, 2013; Werder and others, 2013), and the vertical flow of water within the temperate shear margin. We do not consider sediment transport (Walder and Fowler, 1994; Fowler and Ng, 1996; Creyts and others, 2013), which can alter the channel cross section as the flow rate within an R-channel increases. Antiplane shear increases the creep closure velocity, which requires more melting in the steady state, and therefore, an increase in flow rate through the channel. Sediment transport may in fact play a stabilising role initiating sediment deformation and influencing drainage dynamics (Walder and Fowler, 1994).

The drawbacks to this idealised model highlight several ways in which our analysis may be extended. Here we used a stress-free basal boundary condition along the lower boundary outside of the channel. A frictional sliding law that incorporates subglacial hydrology along the boundary would be more appropriate (Budd and others, 1979; Alley and others, 1986; Perol and others, 2015). In the antiplane direction, adding basal traction would alter the results by increasing the creep closure velocity near the ice/till interface. Depending on the ratio of far-field to basal stress, the shape of the channel would stay closer to circular. It would also be sensible to require frictional sliding in the in-plane direction, i.e. $\sigma_{r\theta}(r, \theta = 0) = g(u_r, N)$, where $g(u_r, N)$ is a sliding law that couples the radial creep velocity u_r to the effective pressure N along the boundary (Weertman, 1972). The radial creep closure is a small quantity and therefore, this traction will likely also be small. Regardless, the additional traction would slow the creep closure at the channel wall and exaggerate the non-circular channel shapes presented in this paper.

To better understand the effect of antiplane shear on the shapes of R-channels, we would perform transient numerical simulations and iteratively evolve the channel surface in time. In preliminary numerical simulations of this form, we find that the channels are not susceptible to a shape instability, which would form due to a reinforced strain concentration at the top of the channel. This is consistent with Dallaston and Hewitt (2014), who show that circular channels can be perturbed to stable ellipses. To fully capture the stability of R-channel shapes, we would also couple the ice flow with heat transfer imparted by the turbulently flowing melt water.

The effects of antiplane shear on the effective pressure in subglacial hydrologic systems could be incorporated into

models as a function of time. For example, we can write a parameterisation for the creep closure velocity as a function of the strain rate ratio S as

$$u_r(r = a) = Aa \left(\frac{N}{n} \right)^n \left[1 + \beta S^{(n-1)/n} \right].$$

This parameterisation reduces to both the small and large S asymptotics with a single parameter β , which represents the large S power-law prefactor. The strain rate ratio S could be written as

$$S = \frac{u_s - u_b}{AhN^n},$$

where the far-field shear strain rate is given as the difference in surface velocity u_s and basal slip velocity u_b divided by $h = H/(n + 1)$, which is the basal shear strain rate in the Nye (1952) solution for glacier flow down a slope in terms of the glacier thickness H divided by the exponent of the vertical coordinate. This parameterisation for S could be incorporated in models for subglacial hydrology such as Hewitt (2011), Bartholomaeus and others (2011) or Werder and others (2013). These models could then be coupled with an ice flow model to capture switches in subglacial drainage and surge initiation (Fowler, 1987; Björnsson, 1998; Oerlemans, 2013).

ACKNOWLEDGEMENTS

We gratefully acknowledge the support from National Science Foundation Graduate Research Fellowship grant number DGE1144152 (CRM), Harvard University School of Engineering and Applied Sciences Blue Hills Hydrology Endowment (MCF), and the National Science Foundation Polar Program grants PP1341499 (JRR) and PP1043481 (TTC). We thank Garry Clarke, Thibaut Perol, John Platt and Christian Schoof for insightful discussions. We also appreciate the helpful suggestions from the scientific editor, Ralf Greve and the anonymous referees.

REFERENCES

- Alley RB, Blankenship DD, Bentley CR and Rooney ST (1986) Deformation of till beneath Ice Stream B, west Antarctica. *Nature*, **322**(6074), 57–59 (doi: 10.1038/322057a0)
- Anderson RS, Hallet B, Walder J and Aubry BF (1982) Observations in a cavity beneath Grinnell Glacier. *Earth Surf. Process. Landforms*, **7**(1), 63–70 (doi: 10.1002/esp.3290070108)
- Barcilon V and Macayeal DR (1993) Steady flow of a viscous ice stream across a no-slip/free-slip transition at the bed. *J. Glaciol.*, **39**(131), 167–185
- Bartholomaeus TC, Anderson RS and Anderson SP (2011) Growth and collapse of the distributed subglacial hydrologic system of Kennicott Glacier, Alaska, USA, and its effects on basal motion. *J. Glaciol.*, **57**(206), 985–1002 (doi: 10.3189/002214311798843269)
- Bentley CR, Lord N and Liu C (1998) Radar reflections reveal a wet bed beneath stagnant Ice Stream C and a frozen bed beneath ridge BC, West Antarctica. *J. Glaciol.*, **44**(146), 149–156
- Björnsson H (1998) Hydrological characteristics of the drainage system beneath a surging glacier. *Nature*, **395**(6704), 771–774
- Blankenship DD, Bentley CR, Rooney ST and Alley RB (1986) Seismic measurements reveal a saturated porous layer beneath an active Antarctic Ice Stream. *Nature*, **322**(6074), 54–57 (doi: 10.1038/322054a0)
- Blankenship DD, Bentley CR, Rooney ST and Alley RB (1987) Till beneath Ice Stream B: 1. Properties derived from seismic travel times. *J. Geophys. Res.*, **92**(B9), 8903–8911 (doi: 10.1029/jb092ib09p08903)
- Boulton GS, Dent DL and Morris EM (1974) Subglacial shearing and crushing, and the role of water pressures in tills from southeast Iceland. *Geogr. Ann.*, **56A**, 135–145
- Brugman MM (1986) *Water flow at the base of a surging glacier*. (PhD thesis, Calif. Inst. of Technol., Pasadena)
- Budd WF, Keage PL and Blundy NA (1979) Empirical studies of ice sliding. *J. Glaciol.*, **23**, 157–170
- Clarke GKC (1987) Subglacial till: a physical framework for its properties and processes. *J. Geophys. Res.*, **92**(B9), 9023–9036 (doi: 10.1029/jb092ib09p09023)
- Clarke GKC (2003) Hydraulics of subglacial outburst floods: new insights from the Spring-Hutter formulation. *J. Glaciol.*, **49**(165), 299–313 (doi: 10.3189/172756503781830728)
- Clarke GKC, Collins SG and Thompson DE (1984) Flow, thermal structure, and subglacial conditions of a surge-type glacier. *Can. J. Earth Sci.*, **21**(2), 232–240 (doi: 10.1139/e84-024)
- Creyts TT and Schoof C (2009) Drainage through subglacial water sheets. *J. Geophys. Res.*, **114**(F04008), 1–18 (doi: 10.1029/2008jf001215)
- Creyts TT, Clarke GKC and Church M (2013) Evolution of subglacial overdeepenings in response to sediment redistribution and glaciohydraulic supercooling. *J. Geophys. Res.*, **118**(2), 423–446 (doi: 10.1002/jgrf.20033)
- Cuffey KM and Paterson WSB (2010) *The physics of glaciers*, 4th edn. Elsevier, Oxford
- Cutler PM (1998) Modelling the evolution of subglacial tunnels due to varying water input. *J. Glaciol.*, **44**(148), 485–497
- Dallaston MC and Hewitt I (2014) Free-boundary models of a melt-water conduit. *Phys. Fluids*, **26**(083101), 1–21 (doi: 10.1063/1.4892389)
- Dassault Systèmes (2012) ABAQUS 6.12-1. Dassault Systèmes
- Durham WB, Kirby SH and Stern LA (1997) Creep of water ices at planetary conditions: a compilation. *J. Geophys. Res.*, **102**(E7), 16293–16302 (doi: 10.1029/97je00916)
- Echelmeyer K and Harrison W (1999) Ongoing margin migration of Ice Stream B, Antarctica. *J. Glaciol.*, **45**(150), 361–369 (doi: 10.3189/002214399793377059)
- Eisen O and 5 others (2005) Variegated Glacier, Alaska, USA: a century of surges. *J. Glaciol.*, **51**(174), 399–406 (doi: 10.3189/172756505781829250)
- Engelhardt H and Kamb B (2013) Kamb Ice Stream flow history and surge potential. *Ann. Glaciol.*, **54**(63), 287–298 (doi: 10.3189/2013aog63a535)
- Engelhardt H, Humphrey N, Kamb B and Fahnestock M (1990) Physical conditions at the base of a fast moving Antarctic ice stream. *Science*, **248**(4951), 57–59 (doi: 10.1126/science.248.4951.57)
- Engelhardt HF and Kamb B (1997) Basal hydraulic system of a West Antarctic ice stream: constraints from borehole observations. *J. Glaciol.*, **43**(144), 207–230
- Engelhardt HF and Kamb B (1998) Basal sliding of Ice Stream B, West Antarctica. *J. Glaciol.*, **44**(147), 223–230
- Eshelby JD (1957) The determination of the elastic field of an ellipsoidal inclusion, and related problems. *Proc. R. Soc. Lond. Ser. A*, **241**(1226), 376–396 (doi: 10.1098/rspa.1957.0133)
- Evatt GW (2015) Röthlisberger channels with finite ice depth and open channel flow. *Ann. Glaciol.*, **50**(70), 45–50 (doi: 10.3189/2015aog70a992)
- Fischer UH and Clarke GKC (1997) Stick slip sliding behaviour at the base of a glacier. *Ann. Glaciol.*, **24**, 390–396
- Flowers GE and Clarke GKC (2002a) A multicomponent coupled model of glacier hydrology 1. Theory and synthetic examples. *J. Geophys. Res.*, **107**(B11), ECV9, 1–17 (doi: 10.1029/2001jb001122)
- Flowers GE and Clarke GKC (2002b) A multicomponent coupled model of glacier hydrology 2. Application to Trapridge Glacier,

- Yukon, Canada. *J. Geophys. Res.*, **107**(B11), ECV-10 (doi: 10.1029/2001jb001124)
- Fountain AG (1993) Geometry and flow conditions of subglacial water at South Cascade Glacier, Washington State, USA: an analysis of tracer injections. *J. Glaciol.*, **39**(131), 143–156
- Fountain AG and Walder JS (1998) Water flow through temperate glaciers. *Rev. Geophys.*, **36**, 299–328 (doi: 10.1029/97rg03579)
- Fowler AC (1987) A theory of glacier surges. *J. Geophys. Res.*, **92**(B9), 9111–9120 (doi: 10.1029/jb092ib09p09111)
- Fowler AC (1989) A mathematical analysis of glacier surges. *SIAM J. Appl. Math.*, **49**(1), 246–263 (doi: 10.1137/0149015)
- Fowler AC (2011) *Mathematical geoscience*, vol. **36**. Springer Science & Business Media, Cambridge, UK
- Fowler AC and Ng FSL (1996) The role of sediment transport in the mechanics of jökulhlaups. *Ann. Glaciol.*, **22**, 255–259
- Fricker HA and Scambos T (2009) Connected subglacial lake activity on lower Mercer and Whillans Ice Streams, West Antarctica, 2003–2008. *J. Glaciol.*, **55**(190), 303–315 (doi: 10.3189/002214309788608813)
- Fricker HA, Scambos T, Bindschadler R and Padman L (2007) An active subglacial water system in West Antarctica mapped from space. *Science*, **315**(5818), 1544–1548 (doi: 10.1126/science.1136897)
- Glen JW (1955) The creep of polycrystalline ice. *Proc. R. Soc. Lond. Ser. A*, **228**(1175), 519–538
- Glen JW (1956) Measurement of the deformation of ice in a tunnel at the foot of an ice fall. *J. Glaciol.*, **2**(20), 735–745
- Goldsby D and Kohlstedt D (2001) Superplastic deformation of ice: experimental observations. *J. Geophys. Res.*, **106**, 11017–11030 (doi: 10.1029/2000jb900336)
- Gray L and 5 others (2005) Evidence for subglacial water transport in the West Antarctic Ice Sheet through three-dimensional satellite radar interferometry. *Geophys. Res. Lett.*, **32**(L03501) (doi: 10.1029/2004gl021387)
- Haefeli R (1951) Some observations on glacier flow. *J. Glaciol.*, **1**(9), 496–500
- Harper JT and 5 others (2001) Spatial variability in the flow of a valley glacier: deformation of a large array of boreholes. *J. Geophys. Res.*, **106**(B5), 8547–8562 (doi: 10.1029/2000jb900440)
- Haseloff M, Schoof C and Gagliardini O (2015) A boundary layer model for ice stream margins. *J. Fluid Mech.*, **781**, 353–387 (doi: 10.1017/jfm.2015.503)
- Henderson FM (1966) *Open channel flow*. MacMillan, New York
- Hewitt IJ (2011) Modelling distributed and channelized subglacial drainage: the spacing of channels. *J. Glaciol.*, **57**(202), 302–314 (doi: 10.3189/002214311796405951)
- Hewitt IJ (2013) Seasonal changes in ice sheet motion due to melt water lubrication. *Earth Planet. Sci. Lett.*, **371**, 16–25 (doi: 10.1016/j.epsl.2013.04.022)
- Hindmarsh RCA (2004) A numerical comparison of approximations to the Stokes equations used in ice sheet and glacier modeling. *J. Geophys. Res.*, **109**(F1) (doi: 10.1029/2003jf000065)
- Hock R and Hooke RL (1993) Evolution of the internal drainage system in the lower part of the ablation area of storglaciaren, sweden. *Geol. Soc. Am. Bull.*, **105**(4), 537–546
- Hooke RL, Laumann T and Kohler J (1990) Subglacial water pressures and the shape of subglacial conduits. *J. Glaciol.*, **36**(122), 67–71
- Hutter K and Olunloyo VOS (1980) On the distribution of stress and velocity in an ice strip, which is partly sliding over and partly adhering to its bed, by using a Newtonian viscous approximation. *Proc. R. Soc. Lond. Ser. A*, **373**(1754), 385–403 (doi: 10.1098/rspa.1980.0155)
- Iken A and Bindschadler RA (1986) Combined measurements of subglacial water pressure and surface velocity of Findelengletscher, Switzerland: conclusions about drainage system and sliding mechanism. *J. Glaciol.*, **32**(110), 101–119
- Joughin I and Tulaczyk S (2002) Positive mass balance of the Ross Ice Streams, West Antarctica. *Science*, **295**(5554), 476–480 (doi: 10.1126/science.1066875)
- Joughin I, Tulaczyk S, Bindschadler R and Price SF (2002) Changes in West Antarctic Ice Stream velocities: observation and analysis. *J. Geophys. Res.*, **107**(B11) (doi: 10.1029/2001jb001029)
- Kamb B (1987) Glacier surge mechanism based on linked cavity configuration of the base water conduit system. *J. Geophys. Res.*, **92**(B9), 9083–9099 (doi: 10.1029/jb092ib09p09083)
- Kamb B (1991) Rheological nonlinearity and flow instability in the deforming bed mechanism of ice stream motion. *J. Geophys. Res.*, **96**(B10), 16585–16595 (doi: 10.1029/91jb00946)
- Kamb B (2001) Basal zone of the West Antarctic Ice Streams and its role in lubrication of their rapid motion. In Alley RB and Bindschadler RA eds. *The West Antarctic ice sheet: behavior and environment*, vol. **77**. AGU, Washington, DC, 157–199 (doi: 10.1029/ar077p0157)
- Kamb B and 7 others (1985) Glacier surge mechanism: 1982–1983 surge of Variegated Glacier, Alaska. *Science*, **227**(4686), 469–479 (doi: 10.1126/science.227.4686.469)
- Kavanaugh JL and Clarke GKC (2000) Evidence for extreme pressure pulses in the subglacial water system. *J. Glaciol.*, **46**(153), 206–212 (doi: 10.3189/172756500781832963)
- Lliboutry L (1968) General theory of subglacial cavitation and sliding of temperate glaciers. *J. Glaciol.*, **7**, 21–58
- Lliboutry L (1979) Local friction laws for glaciers: a critical review and new openings. *J. Glaciol.*, **23**, 67–95
- Ng FSL (1998) *Mathematical modeling of subglacial drainage and erosion*. (PhD thesis, St. Catherine's College, Oxford University)
- Ng FSL (2000) Canals under sediment-based ice sheets. *Ann. Glaciol.*, **30**(1), 146–152 (doi: 10.3189/172756400781820633)
- Nye JF (1952) The mechanics of glacier flow. *J. Glaciol.*, **2**(12), 82–93
- Nye JF (1953) The flow law of ice from measurements in glacier tunnels, laboratory experiments and the Jungfraufirn borehole experiment. *Proc. R. Soc. Lond. Ser. A*, **219**, 477–489
- Nye JF (1973) Water at the bed of a glacier. In *Symposium on the Hydrology of Glaciers, IAHS Publ.*, vol. **95**, 189–194
- Oerlemans J (2013) A note on the water budget of temperate glaciers. *Cryosphere*, **7**, 1557–1564 (doi: 10.5194/tc-7-1557-2013)
- Perol T and Rice JR (2011) Control of the width of West Antarctic ice streams by internal melting in the ice sheet near the margins. In *Abstract C11B-0677 presented at 2011 Fall Meeting, AGU*, San Francisco, CA, 5–9 December
- Perol T and Rice JR (2015) Shear heating and weakening of the margins of West Antarctic ice streams. *Geophys. Res. Lett.*, **42**(9), 3406–3413 (doi: 10.1002/2015gl063638)
- Perol T, Rice JR, Platt JD and Suckale J (2015) Subglacial hydrology and ice stream margin locations. *J. Geophys. Res.*, **120**(F003542), 1–17 (doi: 10.1002/2015jf003542)
- Raymond CF (1987) How do glaciers surge? A review. *J. Geophys. Res.*, **92**(B9), 9121–9134 (doi: 10.1029/jb092ib09p09121)
- Rignot E, Mouginot J and Scheuchl B (2011) Ice flow of the Antarctic ice sheet. *Science*, **333**(6048), 1427–1430 (doi: 10.1126/science.1208336)
- Röthlisberger H (1972) Water pressure in intra- and subglacial channels. *J. Glaciol.*, **11**(62), 177–203
- Sayag R and Tziperman E (2009) Spatiotemporal dynamics of ice streams due to a triple-valued sliding law. *J. Fluid Mech.*, **640**, 483–505 (doi: 10.1017/s0022112009991406)
- Schoof C (2004) On the mechanics of ice-stream shear margins. *J. Glaciol.*, **50**(169), 208–218 (doi: 10.3189/172756504781830024)
- Schoof C (2005) The effect of cavitation on glacier sliding. *Proc. R. Soc. Lond. Ser. A*, **461**(2055), 609–627 (doi: 10.1098/rspa.2004.1350)
- Schoof C (2010a) Coulomb friction and other sliding laws in a higher-order glacier flow model. *Math. Models Methods Appl. Sci.*, **20**(01), 157–189 (doi: 10.1142/s0218202510004180)
- Schoof C (2010b) Ice sheet acceleration driven by melt supply variability. *Nature*, **468**(7325), 803–806 (doi: 10.1038/nature09618)
- Schoof C (2012) Thermally driven migration of ice-stream shear margins. *J. Fluid Mech.*, **712**, 552–578 (doi: 10.1017/jfm.2012.438)

- Schoof C, Rada CA, Wilson NJ, Flowers GE and Haseloff M (2014) Oscillatory subglacial drainage in the absence of surface melt. *Cryosphere*, **8**(3), 959–976 (doi: 10.5194/tc-8-959-2014)
- Shreve RL (1972) Movement of water in glaciers. *J. Glaciol.*, **11**(62), 205–214
- Spring U and Hutter K (1981) Numerical studies of jökulhlaups. *Cold Reg. Sci. Technol.*, **4**(3), 227–244
- Steinemann S (1954) Results of preliminary experiments on the plasticity of ice crystals. *J. Glaciol.*, **2**(16), 404–412
- Suckale J, Platt JD, Perol T and Rice JR (2014) Deformation-induced melting in the margins of the West Antarctic ice streams. *J. Geophys. Res.*, **119**(5), 1004–1025 (doi: 10.1002/2013jfg003008)
- Truffer M and Echelmeyer KA (2003) Of isbrae and ice streams. *Ann. Glaciol.*, **36**(1), 66–72 (doi: 10.3189/172756403781816347)
- Truffer M and Echelmeyer KA (2005) *Margin migration rates and margin dynamics of the Siple Coast ice streams*. National Snow and Ice Data Center, Boulder, CO (doi: <http://dx.doi.org/10.7265/N50K26HH>)
- Tulaczyk S, Kamb B and Engelhardt HF (2000) Basal mechanics of Ice Stream B, West Antarctica: 2. Undrained plastic bed model. *J. Geophys. Res.*, **105**(B1), 483–494 (doi: 10.1029/1999jb900328)
- Tulaczyk S, Kamb B and Engelhardt HF (2001) Estimates of effective stress beneath a modern West Antarctic ice stream from till pre-consolidation and void ratio. *Boreas*, **30**(2), 101–114 (doi: 10.1080/03009480120262)
- Vogel SW and 7 others (2005) Subglacial conditions during and after stoppage of an Antarctic Ice Stream: is reactivation imminent? *Geophys. Res. Lett.*, **32** (doi: 10.1029/2005gl022563)
- Walder J and Hallet B (1979) Geometry of former subglacial water channels and cavities. *J. Glaciol.*, **23**, 335–346
- Walder JS (1986) Hydraulics of subglacial cavities. *J. Glaciol.*, **32** (112), 439–445
- Walder JS and Fowler AC (1994) Channelized subglacial drainage over a deformable bed. *J. Glaciol.*, **40**(134), 3–15
- Weertman J (1972) General theory of water flow at base of a glacier or ice sheet. *Rev. Geophys. Space Phys.*, **10**, 287–333 (doi: 10.1029/rg010i001p00287)
- Werder MA, Hewitt IJ, Schoof C and Flowers GE (2013) Modeling channelized and distributed subglacial drainage in two dimensions. *J. Geophys. Res.*, **118**(F20146), 1–19 (doi: 10.1002/jgrf.20146)

APPENDIX A

Equation (25) is a linear, equidimensional equation. We therefore try for a solution of the form

$$U_x = R^\lambda f(\theta).$$

Inserting this ansatz, we find the equation

$$\lambda[\lambda + 2 - (2/n)]f(\theta) + f''(\theta) = 0.$$

Thus,

$$f(\theta) = A \sin\left(\sqrt{\lambda[\lambda + 2 - (2/n)]}\theta\right) + B \cos\left(\sqrt{\lambda[\lambda + 2 - (2/n)]}\theta\right).$$

By symmetry, the velocity is mirrored across the y -axis ($\Sigma_{\theta x}(r; \theta = 0) = \partial U_x / \partial \theta = 0$) and therefore, the solution is proportional to $\cos(\theta)$. Next we require the solution to be periodic over $0 \leq \theta \leq 2\pi$, as in

$$\sqrt{\lambda[\lambda + 2 - (2/n)]} = k, \quad \text{where } k = 0, 1, 2, 3, \dots$$

Hence, the eigenvalues are

$$\lambda_k = (1 - n)/n \pm \sqrt{[1 - (1/n)]^2 + k^2}. \quad (A1)$$

The full solution can then be written as an infinite series

$$U_x = \sum_{k=0}^{\infty} \left[a_k R^{(1-n)/n + \sqrt{[1 - (1/n)]^2 + k^2}} + b_k R^{(1-n)/n - \sqrt{[1 - (1/n)]^2 + k^2}} \right] \cos(k\theta).$$

The boundary conditions are

$$\left. \frac{\partial U_x}{\partial \theta} \right|_{\theta=0} = 0, \quad \left. \frac{\partial U_x}{\partial R} \right|_{R=1} = 0 \quad \text{and} \quad U_x(R = B) = B \cos(\theta).$$

The first condition is satisfied due to symmetry. Setting $k = 1$ and defining the positive root of the eigenvalue λ_1 , as λ_+ and the negative λ_- , we can write the third condition as

$$a_1 B^{\lambda_+} + b_1 B^{\lambda_-} = B.$$

The second boundary condition then gives

$$\left. \frac{\partial U_x}{\partial R} \right|_{R=1} = a_1 \lambda_+ + b_1 \lambda_- = 0.$$

Solving for b_1 we have

$$b_1 = -\frac{a_1 \lambda_+}{\lambda_-}.$$

Hence, we find that

$$a_1 = \frac{B/\lambda_+}{(B^{\lambda_+}/\lambda_+) - (B^{\lambda_-}/\lambda_-)} \cos(\theta),$$

$$b_1 = \frac{-B/\lambda_-}{(B^{\lambda_+}/\lambda_+) - (B^{\lambda_-}/\lambda_-)} \cos(\theta).$$

Now we can write the full solution as

$$U_x = B \frac{(R^{\lambda_+}/\lambda_+) - (R^{\lambda_-}/\lambda_-)}{(B^{\lambda_+}/\lambda_+) - (B^{\lambda_-}/\lambda_-)} \cos(\theta).$$

MS received 22 December 2015 and accepted in revised form 11 April 2016; first published online 16 May 2016